ON ITERATIVE SOLUTIONS FOR NUMERICAL COLLISION MODELS

Vasileios Chatziioannou
Department of Music Acoustics,
University of Music and
performing Arts Vienna, Austria
chatziioannou@mdw.ac.at

Sebastian Schmutzhard
Department of Music Acoustics,
University of Music and
performing Arts Vienna, Austria
schmutzhard@mdw.ac.at

Stefan Bilbao
Acoustics and Audio Group,
University of Edinburgh
Edinburgh, UK
sbilbao@staffmail.ed.ac.uk

ABSTRACT

Nonlinear interactions between different parts of musical instruments present several challenges regarding the formulation of reliable and efficient numerical sound synthesis models. This paper focuses on a numerical collision model that incorporates impact damping. The proposed energy-based approach involves an iterative solver for the solution of the nonlinear system equations. In order to ensure the efficiency of the presented algorithm a bound is derived for the maximum number of iterations required for convergence. Numerical results demonstrate energy conservation as well as convergence within a small number of iterations, which is usually much lower than the predicted bound. Finally, an application to music acoustics, involving a clarinet simulation, shows that including a loss mechanism during collisions may have a significant effect on sound production.

1. INTRODUCTION

Collisions inherently take place during sound production from musical instruments [1]. Recent attempts have been therefore made in order to incorporate numerical collision models to physics-based sound synthesis algorithms [2, 3, 4]. The prevalent approach towards efficient schemes that may cover the whole audio range is to use time-stepping algorithms, such as the finite difference method [5], digital waveguides [6] and modal-based approaches [7, 8]. This requires discrete-time modelling of nonlinear interactions, a problem that gives rise to several challenges, such as existence and uniqueness of solutions to the underlying nonlinear equations, as well as the guarantee of numerical stability.

Although impact losses are often neglected in music acoustics applications, it has been proposed to include this effect by using the Hunt-Crossley impact model [3, 9, 10, 11]. Such a practise may result in minor, yet acoustically significant alterations of the synthesised sounds, as will be shown in Section 4. The accuracy of numerical solutions to this model equations has been the subject of a recent study [12], where a correction-based method was proposed to accurately approximate the velocity of impacting objects, based on enforcing numerical energy consistency. In the present work a solver is employed, that is shown to provide approximations of high accuracy, without the need of a post-processing step. Furthermore, since iterative solvers are employed in order to numerically solve the (nonlinear) model equations, special attention is devoted to the convergence speed of the algorithm, by calculating the maximum number of required iterations. Convergence within a given number of iterations is particularly useful in applications where an efficient solver is sought after, as for example real-time sound synthesis.

Section 2 presents the Hunt-Crossley impact model, along with an energy-based numerical formulation. Section 3 incorporates this model to the simulation of a damped harmonic oscillator, with or without the presence of external forces. An iterative solution is carried out, for which a bound on the number of required iterations is calculated. Section 4 presents an application of the formulated model to musical instruments, in terms of a clarinet tone simulation and Section 5 discusses the findings of the current study in the context of acoustics research.

2. IMPACT MODELING

Consider a mass approaching a rigid barrier from below, with contact occurring at $y = 0$. The Hunt-Crossley repelling force can be defined as

$$f_\mathrm{c} = -k_\mathrm{c} \lfloor y \rfloor^\alpha - \lambda_\mathrm{c} \lfloor y \rfloor^\alpha \frac{\mathrm{d}y}{\mathrm{d}t}, \tag{1}$$

where $\lfloor y \rfloor^\alpha = h(y) y^\alpha$, $\alpha \geq 1$ is a power-law exponent and $h(y)$ denotes the Heaviside step function. This non-negative term represents the compression of the mass while in contact with the barrier [2, 10, 13], a model which has been shown to be in agreement with experimental measurements in musical instruments [14, 15, 16].[1] The constant k_c represents stiffness and λ_c is a damping constant. The negative sign indicates that this force is acting against the motion of the mass 'through' the barrier. Newton's second law can be used to derive the equation of motion of the system

$$m \frac{\mathrm{d}^2 y}{\mathrm{d}t^2} = f_\mathrm{c}, \tag{2}$$

where m represents mass. For this system of lumped contact Papetti et al. [12] derived an analytic expression for the energy H as a function of the velocity v, which reads

$$H(v) = \frac{m}{2} v^2 - \frac{m}{r}(v - v_\mathrm{im}) + \frac{m}{r^2} \ln \left| \frac{1 + rv}{1 + r v_\mathrm{im}} \right|, \tag{3}$$

where v_im is the velocity with which the mass hits the barrier (impact velocity) and $r = \lambda_\mathrm{c}/k_\mathrm{c}$ is a damping factor. This formula may be used to compare numerically obtained results with an analytical solution.

An energy-based formulation of the system may be derived by defining the collision potential

$$V_\mathrm{c} = \frac{k_\mathrm{c}}{\alpha + 1} \lfloor y \rfloor^{\alpha+1}. \tag{4}$$

The collision force can then be written as [13]

$$f_\mathrm{c} = -\frac{\partial V_\mathrm{c}}{\partial y} - r \frac{\partial V_\mathrm{c}}{\partial t}. \tag{5}$$

[1] Note that in cases where the collision is assumed to be rigid (see, e.g. [4, 8]), this term corresponds to an artificial penalisation.

Following [10] (2) is cast into Hamiltonian form as

$$\frac{\mathrm{d}y}{\mathrm{d}t} = \frac{\partial T}{\partial p} \tag{6a}$$

$$\frac{\mathrm{d}p}{\mathrm{d}t} = -\frac{\partial V_\mathrm{c}}{\partial y} - r\frac{\partial V_\mathrm{c}}{\partial t}, \tag{6b}$$

where $T = p^2/(2m)$ represents the kinetic energy, p being the conjugate momentum. Similar formulations, including losses within an energy balanced framework, have been recently derived using a port-Hamiltonian formulation (see, e.g. [17]).

2.1. Numerical formulation

System (6) can be discretised by employing mid-point derivative approximations for all terms (see, e.g. [2, 3]). The approximation to the continuous variable $y(t)$ at time $n\Delta t$, where Δt is the sampling interval, is denoted by y^n. Then (6) is discretised as

$$\frac{y^{n+1} - y^n}{\Delta t} = \frac{T(p^{n+1}) - T(p^n)}{p^{n+1} - p^n} \tag{7a}$$

$$\frac{p^{n+1} - p^n}{\Delta t} = -\frac{V_\mathrm{c}(y^{n+1}) - V_\mathrm{c}(y^n)}{y^{n+1} - y^n} - r\frac{V_\mathrm{c}(y^{n+1}) - V_\mathrm{c}(y^n)}{\Delta t}. \tag{7b}$$

Defining the normalised momentum $q^n = p^n\Delta t/(2m)$ yields

$$y^{n+1} - y^n = q^{n+1} + q^n \tag{8a}$$

$$q^{n+1} - q^n = -\frac{\Delta t^2}{2m}\frac{V_\mathrm{c}(y^{n+1}) - V_\mathrm{c}(y^n)}{y^{n+1} - y^n} - r\frac{\Delta t}{2m}\left(V_\mathrm{c}(y^{n+1}) - V_\mathrm{c}(y^n)\right). \tag{8b}$$

Using the auxiliary variable $x = y^{n+1} - y^n$ leads to the following nonlinear equation in x

$$F(x) = x - 2q^n + \frac{\Delta t^2}{2m}\frac{V_\mathrm{c}(y^n + x) - V_\mathrm{c}(y^n)}{x} + r\frac{\Delta t}{2m}\left(V_\mathrm{c}(y^n + x) - V_\mathrm{c}(y^n)\right) = 0. \tag{9}$$

Note that

$$\lim_{x\to 0} F(x) = \frac{\Delta t^2}{2m}V_\mathrm{c}'(y^n) - 2q^n, \tag{10}$$

where V_c' signifies taking the derivative of V_c with respect to position. This can be used to avoid singularities in $F(x)$. Equation (9) can be solved using, e.g. the Newton-Raphson or the bisection method. A bound on the required number of iterations for these methods can be obtained as shown in Section 3.3. Existence and uniqueness of solutions for (9) can be proven, as explained in [2], using the convexity of V_c and the positivity of V_c' which imply that $F' \geq 1$ and $F'' \geq 0$. Displacement and momentum can be subsequently updated using

$$y^{n+1} = x + y^n$$
$$q^{n+1} = x - q^n, \tag{11}$$

whence p^{n+1} is also obtained. For energy conserving (Hamiltonian) systems this method can be shown to conserve the numerical energy within machine precision in implementations on digital processors [13] and is hence labelled EC for the remainder of this text.

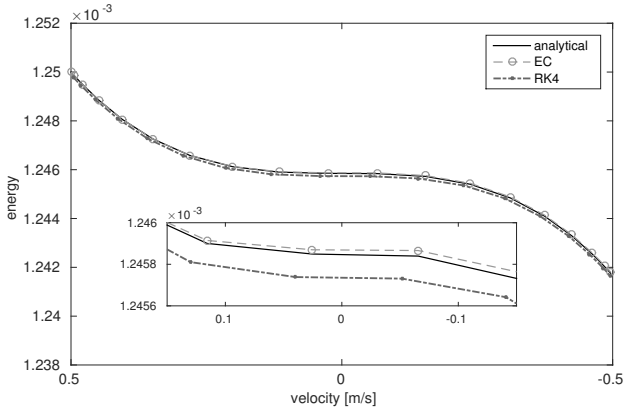

Figure 1: Simulation of a mass colliding with a barrier, using the Hunt-Crossley model. The system energy of the presented method and the fourth order Runge-Kutta method during the impact is compared to the continuous (analytical) solution from (3). A zoomed area shows a more clearer comparison of the approximation methods.

Following [12] the presented method is compared to the analytical solution (3) and to a higher order approximation given by a fourth order Runge-Kutta method (RK4). Figure 1 shows the energy during the impact as a function of the compression velocity. The parameters' values used for the simulations (listed in Table 1) are taken from [12]. It can be observed that the EC method accurately reproduces the analytical result, outperforming the higher-order Runge-Kutta method. This is a result of the exact energy-conserving nature of this algorithm, in the case of Hamiltonian systems, that is projected here to a dissipative case.

Table 1: Parameters used in the impact model.

mass	$m = 0.01$ kg
stiffness constant	$k_\mathrm{c} = 10^7$ N/m$^\alpha$
damping factor	$r = 0.01$ s/m
exponent	$\alpha = 1.3$
impact velocity	$v_\mathrm{im} = 0.5$ m/s
sampling rate	$f_s = 44100$ Hz

3. DAMPED OSCILLATOR WITH CONTACT

The above impact model can be readily incorporated to the simulation of a damped oscillator. Consider a mass-spring system with stiffness $k = m(2\pi f_0)^2$, f_0 being the resonance frequency of the oscillator. The potential energy is now given by $V = V_s + V_\mathrm{c}$, where $V_s = ky^2/2$ and V_c is the collision potential of the previous section. A damping term is also included in the equation of motion of the system (see Figure 2), which reads

$$m\frac{\mathrm{d}^2y}{\mathrm{d}t^2} + m\gamma\frac{\mathrm{d}y}{\mathrm{d}t} + ky + k_\mathrm{c}\lfloor y\rfloor^\alpha\left(1 + r\frac{\mathrm{d}y}{\mathrm{d}t}\right) = 0, \tag{12}$$

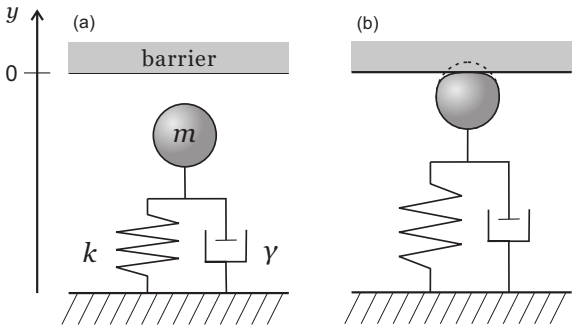

Figure 2: Sketch of a damped harmonic oscillator (a) before and (b) during contact with the barrier.

γ being a damping factor. This system can be written in Hamiltonian form as [10]

$$\frac{\mathrm{d}y}{\mathrm{d}t} = \frac{\partial T}{\partial p} \tag{13a}$$

$$\frac{\mathrm{d}p}{\mathrm{d}t} = -\frac{\partial V}{\partial y} - r\frac{\mathrm{d}V_\mathrm{c}}{\mathrm{d}t} - \gamma p. \tag{13b}$$

For the evolution of the system energy $H = T + V$ the following expression can be derived

$$\begin{aligned}\frac{\mathrm{d}H}{\mathrm{d}t} &= \frac{\partial H}{\partial y}\frac{\mathrm{d}y}{\mathrm{d}t} + \frac{\partial H}{\partial p}\frac{\mathrm{d}p}{\mathrm{d}t} = -\frac{\gamma p^2}{m} - \frac{rp}{m}\frac{\mathrm{d}V_\mathrm{c}}{\mathrm{d}t} \\ &= -\frac{p^2}{m^2}\left(m\gamma + rk_\mathrm{c}\lfloor y\rfloor^\alpha\right) \leq 0,\end{aligned} \tag{14}$$

which is in accordance with both loss mechanisms, with the energy decreasing due to frictional forces. In search of an invariant quantity, the following conservation law can thus be derived [18]

$$H + \int \frac{\gamma p^2}{m}\mathrm{d}t + \int \frac{rp}{m}\mathrm{d}V_\mathrm{c} = \text{const.} \tag{15}$$

The numerical formulation of (13), using the EC discretisation method, is

$$\frac{y^{n+1} - y^n}{\Delta t} = \frac{T(p^{n+1}) - T(p^n)}{p^{n+1} - p^n} \tag{16a}$$

$$\begin{aligned}\frac{p^{n+1} - p^n}{\Delta t} = &-\frac{V(y^{n+1}) - V(y^n)}{y^{n+1} - y^n} \\ &- r\frac{V_\mathrm{c}(y^{n+1}) - V_\mathrm{c}(y^n)}{\Delta t} - \gamma\mu_{t+}p^n,\end{aligned} \tag{16b}$$

where $\mu_{t+}p^n = (p^{n+1} + p^n)/2$. This leads to the solution of a nonlinear equation in x (again for $x = y^{n+1} - y^n$)

$$\begin{aligned}F(x) = &(1 + \gamma\frac{\Delta t}{2})x - 2q^n + \frac{\Delta t^2}{4m}k(x + 2y^n) \\ &+ \frac{\Delta t^2}{2m}\frac{k_\mathrm{c}}{\alpha+1}\frac{\lfloor y^n + x\rfloor^{\alpha+1} - \lfloor y^n\rfloor^{\alpha+1}}{x} \\ &+ r\frac{\Delta t}{2m}\frac{k_\mathrm{c}}{\alpha+1}\left(\lfloor y^n + x\rfloor^{\alpha+1} - \lfloor y^n\rfloor^{\alpha+1}\right) = 0.\end{aligned} \tag{17}$$

Note that proving existence and uniqueness of solutions, as well as avoiding singularities can be shown in a similar fashion as for (9).

3.1. Energy balance

In musical instrument simulation, such lumped oscillators, representing the vibroacoustical behaviour of an instrument, are often driven by external forces due to interacting objects or acoustic pressure. Given such an external force f_ex, equation (13b) transforms into

$$\frac{\mathrm{d}p}{\mathrm{d}t} = -\frac{\partial V}{\partial y} - r\frac{\mathrm{d}V_\mathrm{c}}{\mathrm{d}t} - \gamma p + f_\mathrm{ex}, \tag{18}$$

which causes (17) to transform into

$$F(x) - \frac{\Delta t^2}{2m}\mu_{t+}f_\mathrm{ex}^n = 0. \tag{19}$$

The energy balance accordingly becomes

$$\frac{\mathrm{d}H}{\mathrm{d}t} = \frac{pf_\mathrm{ex}}{m} - \frac{p^2}{m^2}\left(m\gamma + rk_\mathrm{c}\lfloor y\rfloor^\alpha\right). \tag{20}$$

Note that the energy is, in general, not monotonically decreasing any more, due to the power supplied by the external force, hence the system is not dissipative. However, in the absence of excitation (when the external force $f_\mathrm{ex} = 0$) the energy is continuously decreasing, since $\mathrm{d}H/\mathrm{d}t \leq 0$ and the system is dissipative. Discretising (20) yields

$$\begin{aligned}\frac{H^{n+1} - H^n}{\Delta t} = &-\frac{\gamma}{m}(\mu_{t+}p^n)^2 - \frac{r}{m}\mu_{t+}p^n\frac{V_\mathrm{c}^{n+1} - V_\mathrm{c}^n}{\Delta t} \\ &+ \frac{\mu_{t+}p^n}{m}\mu_{t+}f_\mathrm{ex}^n,\end{aligned} \tag{21}$$

with $H^n = T(p^n) + V(y^n)$. This induces the following discrete conservation law [18]

$$\begin{aligned}&H^{n+1} + \sum_{\kappa=0}^{n}\frac{\mu_{t+}p^\kappa}{m}\left(\gamma\mu_{t+}p^\kappa + r\frac{V_\mathrm{c}^{\kappa+1} - V_\mathrm{c}^\kappa}{\Delta t} - \mu_{t+}f_\mathrm{ex}^n\right)\Delta t \\ &= K^n = \text{const.}\end{aligned} \tag{22}$$

3.2. Bounds on the discrete solution

The magnitude of the numerical approximations for q^n and y^n can be bound in regard to the initial energy of the system, the external force and the model parameters. Since

$$\begin{aligned}\mu_{t+}p^n\frac{V_c^{n+1} - V_c^n}{\Delta t} &= \mu_{t+}p^n\frac{V_c^{n+1} - V_c^n}{y^{n+1} - y^n}\frac{y^{n+1} - y^n}{\Delta t} \\ &= \frac{(\mu_{t+}p^n)^2}{m}V_c'(y) \geq 0,\end{aligned} \tag{23}$$

it follows from (22) that

$$H^{n+1} \leq H^n - \Delta t\frac{\gamma}{m}\left(\mu_{t+}p^n\right)^2 + \Delta t\frac{\mu_{t+}p^n}{m}\mu_{t+}f_\mathrm{ex}^n. \tag{24}$$

The parabola $-\gamma z^2 + z\mu_{t+}f_\mathrm{ex}^n$ attains its maximum at $z = \mu_{t+}f_\mathrm{ex}^n/(2\gamma)$, hence we obtain the estimate

$$H^{n+1} \leq H^n + \frac{\Delta t}{m}\frac{(\mu_{t+}f_\mathrm{ex}^n)^2}{4\gamma}. \tag{25}$$

Using the facts that $0 \leq \frac{p^2}{2m}, \frac{ky^2}{2} \leq H$, $q = p\dfrac{\Delta t}{2m}$ and $x = q^{n+1} + q^n$, the following local estimate for the solution of $F(x) = 0$ is obtained

$$\left|q^{n+1}\right| \leq \frac{\Delta t}{2m}\sqrt{2mH^n + \frac{\Delta t}{2\gamma}\left(\mu_{t+} f_{\text{ex}}^n\right)^2}. \tag{26}$$

Assuming an upper bound on the external force, $f_{\text{ex}}^{\max}$, one can also obtain the global estimate for times smaller than a final time $t_{\text{end}} \geq (n+1)\Delta t$

$$H^{n+1} \leq H^0 + \frac{t_{\text{end}}}{m}\frac{\left(f_{\text{ex}}^{\max}\right)^2}{4\gamma}, \tag{27}$$

which leads, for $\gamma > 0$ to

$$\left|q^{n+1}\right| \leq \frac{\Delta t}{2m}\sqrt{2mH^0 + t_{\text{end}}\frac{\left(f_{\text{ex}}^{\max}\right)^2}{2\gamma}} \tag{28a}$$

$$|x| \leq \frac{\Delta t}{m}\sqrt{2mH^0 + t_{\text{end}}\frac{\left(f_{\text{ex}}^{\max}\right)^2}{2\gamma}} := B_x \tag{28b}$$

and for the solution y^{n+1}, we obtain for $k > 0$ the following estimate

$$\left|y^{n+1}\right| \leq \sqrt{\frac{2H^0}{k} + t_{\text{end}}\frac{\left(f_{\text{ex}}^{\max}\right)^2}{2mk\gamma}} := B_y. \tag{29}$$

Note that for $\gamma = 0$ and $f_{\text{ex}} = 0$ (as is the case in Figure 4) these bounds can be shown to be equal to $B_x = \frac{\Delta t}{m}\sqrt{2mH^0}$ and $B_y = \sqrt{\frac{2H^0}{k}}$.

3.3. Bound on the number of iterations

One common issue when using iterative methods to solve nonlinear equations is the number of iterations required for the numerical solution to converge. Indeed, for certain parameter choices similar iterative schemes may fail to converge, as reported in [7]. Therefore a formal calculation is presented here for the maximum number of iterations required for the numerical solution of (19) using Newton's method (or alternatively the bisection method).

In the presence of an external force, the uniqueness of the solution of $F(x) = 0$ needs to be analysed separately. Assuming uniqueness, the bisection method halves the interval whose mean is an approximation to the solution of $F(x) = 0$ in each iteration. From the bound (28b) on x therefore it follows that it takes at most

$$k = \log_2 \frac{B_x}{\varepsilon} \tag{30}$$

iterations for the bisection method to converge up to precision ε, when starting within the interval $[-B_x, B_x]$.

Uniqueness can be guaranteed when the external force does not depend on the state (y and y') of the oscillator, hence f_{ex}^{n+1} is a function independent of x. Under this assumption, one can show that

$$F'(x) \geq 1, \tag{31}$$

$$F''(x) \geq 0, \tag{32}$$

and use these facts for the analysis of Newton's method. This leads (see Appendix) to the fact that in order to achieve a given precision ε in the approximation of the unique solution x^* of $F(x) = 0$, one needs to perform at most k Newton iterations when starting from $x_0 \geq x^*$ and $k+1$ iterations when starting from $x_0 < x^*$, with

$$k = \frac{\log\varepsilon - \log(2B_x)}{\log\left(1 - \frac{1}{F'(B_x, B_y)}\right)}. \tag{33}$$

When f_{ex} depends on (y, y') but a bound on its magnitude is known, then existence and uniqueness can also be guaranteed for Δx being small enough. Note that both bounds (for the bisection and Newton's method) constitute a worst-case-scenario estimation and, as shown in Figures 3 and 4 below, convergence is expected to occur earlier. It is still advisable however to ensure that such bounds exist.

3.4. Numerical results

Figures 3 and 4 show simulation examples for a damped, driven oscillator and an undamped oscillator, both undergoing repeated collisions including impact damping. Figure 3(b) demonstrates the conservation law (22) by plotting the error

$$e^n = \frac{K^n - K^0}{\mathcal{P}_{\in}(K^0)} \tag{34}$$

for a system with resonance frequency $f_0 = 3000$ Hz, where $\mathcal{P}_{\in}(K^0) \leq K^0$ is the nearest power of two to K^0 from the left [19]. The external driving force is a sinusoid with a 440 Hz frequency. The other model parameters are the same as in Section 2 and the initial conditions are $y^0 = -0.1$ mm; $p^0 = 0.005$ kg m/s. The dashed line in Figure 3(a) shows the mass displacement in the absence of the external force. Figure 3(c) shows how many Newton iterations are required at each time step for convergence to machine precision. These are well below the theoretical bound calculated in Section 3.3, which is equal to 12 iterations for Newton's method and 38 iterations for the bisection method; note however that the bisection method requires less operations at each iteration. Figure 4 presents the case where the external force and the linear damping are omitted ($\gamma = 0$), and the impact damping factor r is increased 500 times to exaggerate its effect. It can be observed that in both cases K^n is conserved within machine precision and Newton's method converges quite fast, which can be explained by the presence of a good starting point for x, available from the solution at the previous time step.

Figure 5 shows how the number of iterations may increase when an arbitrary starting point is chosen. This starting point is enforced for all time-steps during a 10 ms long simulation, using the same parameters as in Figure 3. The maximum number of required iterations across all time-steps is plotted for each chosen starting point value. Since $F'(x) \geq 1$ and $F''(x) \geq 0$ only a poor starting point larger than B_x will result in slower convergence rates[2], as explained in the Appendix.

[2] In practice, using the solution at the previous time-step as a starting point guarantees that $x_0 \in [-B_x, B_x]$. However, depending on the shape of $F(x)$, x_1 may indeed lie on the right hand side of B_x. In that case one should set $x_1 = B_x$, since the solution x^* is expected to lie in $[-B_x, B_x]$. When generating Figure 5, starting from an arbitrary x_0, this substitution was not carried out, in order to demonstrate the possibility of slow convergence rates in the absence of a bound on the discrete solution.

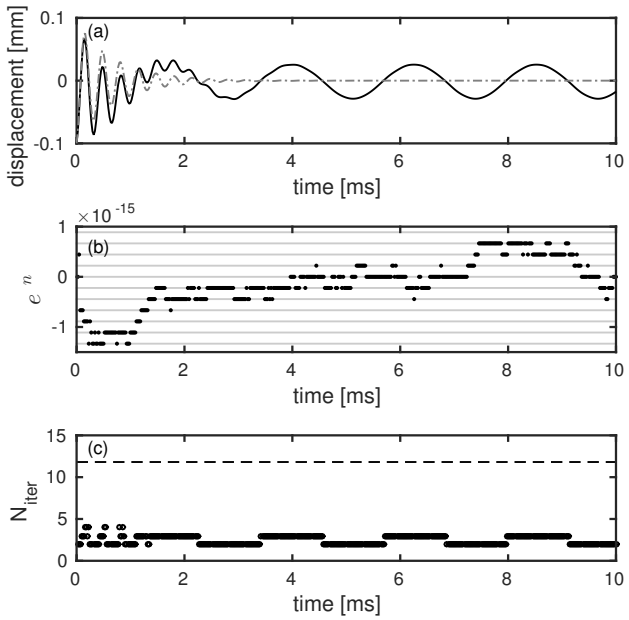

Figure 3: Simulation of a damped, driven oscillator involving multiple impacts modeled using the Hunt-Crossley approach ($\gamma = 3000\ \mathrm{s}^{-1}$, $r = 0.01$ s/m). (a): mass displacement (the dashed line shows the displacement in the absence of the external force). (b): error in the conservation of K^n. Horizontal lines indicate multiples of single bit variation. (c): Number of iterations required for Newton's method to converge (the dashed line indicates the theoretical bound on the number of iterations).

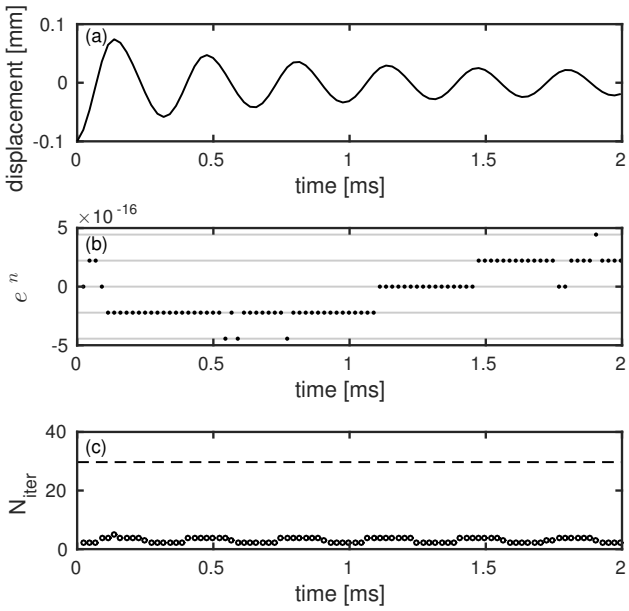

Figure 4: Simulation of an undamped oscillator involving multiple impacts modeled using the Hunt-Crossley approach ($\gamma = 0$, $r = 5$ s/m). (a): mass displacement. (b): error in the conservation of K^n. Horizontal lines indicate multiples of single bit variation. (c): Number of iterations required for Newton's method to converge (the dashed line indicates the theoretical bound on the number of iterations).

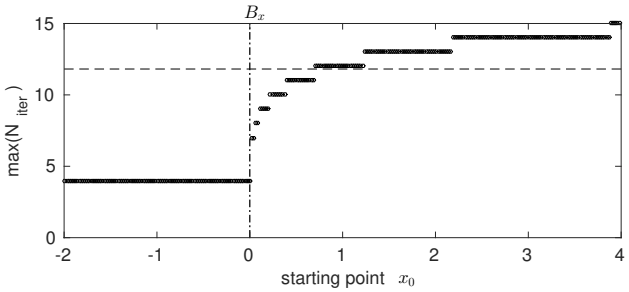

Figure 5: The maximum number of required iterations for different choices of the starting point x_0 for the Newton solver. The horizontal dashed line indicates the theoretical bound on the number of iterations and the vertical one shows the limit that should be enforced on x_1 in order for the iteration bound to be valid (see Appendix; in this case $B_x = 4.42 \cdot 10^{-5}$). Evidently such a limit was not enforced in this numerical experiment.

4. APPLICATION TO SOUND SYNTHESIS

An application of the above damping model is demonstrated in this section using a problem from music acoustics. In particular, the motion of a clarinet reed is simulated and the resulting sound is synthesised. The clarinet reed is driven by the pressure difference across it $p_\Delta = p_\mathrm{m} - p_\mathrm{in}$, where p_m is the blowing pressure and p_in is the pressure inside the clarinet mouthpiece. Hence the force applied to the reed due to the pressure difference is $f_\Delta = S_\mathrm{r} p_\Delta$, where S_r is the effective reed area [20]. Thus the motion of the reed is governed by [3]

$$m\frac{\mathrm{d}^2 y}{\mathrm{d}t^2} + m\gamma\frac{\mathrm{d}y}{\mathrm{d}t} + ky + k_\mathrm{c}\lfloor (y - y_\mathrm{c})\rfloor^\alpha \left(1 + r\frac{\mathrm{d}y}{\mathrm{d}t}\right) = f_\Delta. \quad (35)$$

Two distinct nonlinearities take place here. The first one is due to the collision of the reed with the mouthpiece lay and is modelled using the collision potential defined in Section 2. This nonlinear reed-lay interaction becomes effective after the reed displacement y exceeds a certain value y_c [21, 22] and hence an offset is required inside the 'beating bracket' defined under equation (1). The second nonlinearity stems from the relationship between mouthpiece pressure p_in and mouthpiece flow u_in. The flow is built up from two components [3, 22], the Bernoulli flow u_f and the flow u_r induced by the motion of the reed, with

$$u_\mathrm{in} = u_\mathrm{f} + u_\mathrm{r} \quad (36a)$$

$$u_\mathrm{f} = \sigma w h \sqrt{\frac{2|p_\Delta|}{\rho}} \quad (36b)$$

$$u_\mathrm{r} = S_\mathrm{r}\frac{\mathrm{d}y}{\mathrm{d}t}, \quad (36c)$$

where $\sigma = \mathrm{sign}(p_\Delta)$, ρ is the air density, w the width of the reed

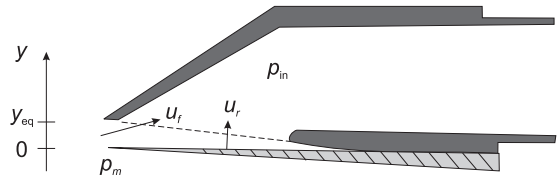

Figure 6: Sketch of the single-reed–mouthpiece system. y_{eq} is the equilibrium position of the reed, u_{f} and u_{r} the Bernoulli and reed flow respectively and p_{m} and p_{in} the mouth pressure and mouthpiece pressure.

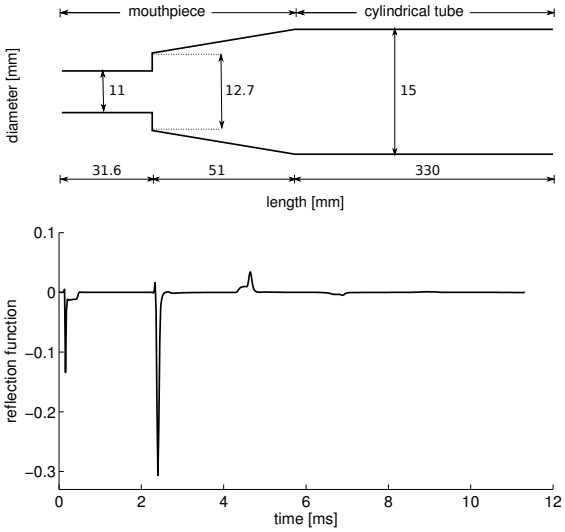

Figure 7: Top: schematic profile of a simplified clarinet bore (not to scale). Bottom: the simulated reflection function.

and $h = y_{\mathrm{eq}} - y$ the reed opening, y_{eq} being the equilibrium opening of the reed after the player positions his lip (see [23]). These parameters, related to the single-reed excitation mechanism, are visualized in Figure 6. Note that in principle h is allowed to become negative, something avoided in the simulations presented here, due to the effect of the collision force. Nevertheless, it is safer to define $h = \lfloor y_{\mathrm{eq}} - y \rfloor$, in order to allow an arbitrary variation of model parameters that might affect the reed opening.

The mouthpiece pressure can be obtained using convolution with the reflection function of the tube [22]. The geometry of the tube (including the mouthpiece) used in the numerical simulations is shown in Figure 7. Its input impedance was calculated using the Acoustics Research Tool [24], including viscothermal losses at the walls and radiation losses at the open end. This can be converted to the reflection function of the tube (also plotted in Figure 7) following the procedure described in [25]. An energy balance for such a coupled system has been explored in [3] where the air column is also discretised using the finite difference method.

The effect of including the impact damping in the single-reed model is visualized in Figure 8 where the spectrogram of the mouthpiece pressure p_{in} is compared to that of the same simulation but with the impact damping omitted. The model parameters used in the simulations are given in Table 2. It can be observed that taking impact damping into account results in the dissipation of higher

Table 2: Physical model parameters used in the clarinet simulation.

reed surface	$S_{\mathrm{r}} = 9.856 \cdot 10^{-5}$ m^2
stiffness/area	$k/S_{\mathrm{r}} = 1.792 \cdot 10^{7}$ Pa/m
equilibrium	$y_{\mathrm{eq}} = 4.09 \cdot 10^{-4}$ m
blowing pressure	$p_{\mathrm{m}} = 3637$ Pa
reed width	$\lambda = 0.012$ m
reed mass/area	$m/S_{\mathrm{r}} = 0.0332$ kg/m^2
damping	$\gamma = 3000$ 1/s
impact stiffness/area	$k_{\mathrm{c}}/S_{\mathrm{r}} = 2 \cdot 10^{10}$ Pa/m$^{\alpha}$
impact damping	$r = 1$ s/m
impact exponent	$\alpha = 2$

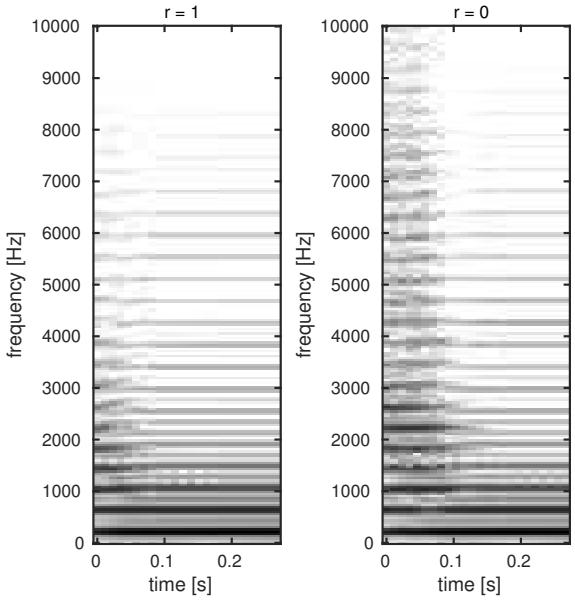

Figure 8: Spectrogram of the simulated mouthpiece pressure p_{in} with (left) and without impact damping (right).

harmonics, especially during the transient. The parameters related to this loss mechanism are here chosen arbitrarily; they are expected to vary depending on the type of reed used (plastic reeds have seen increased use lately) and the material properties and exact geometry of the mouthpiece lay. The latter is often specified by musicians as having a significant effect on the response of the instrument.

5. DISCUSSION

A power balance model for impact damping has been presented. This leads to the numerical solution of a nonlinear equation, with Newton's method being a suitable solver. The fact that such equations need to be solved iteratively led to an efficiency analysis in terms of the maximum number of iterations required for convergence. Note that such a limit represents a worst-case scenario. Convergence is usually achieved earlier, due to the presence of a good starting point for the solver, which is given by the solution at the previous time step. Nevertheless, the presented analysis pro-

vides a guarantee that simulation algorithms will always converge within a given number of iterations steps.

Including impact damping when modelling object collisions, a quantity that is often neglected in sound synthesis applications, appears to have a significant effect on certain systems. This is illustrated by a simulation of a clarinet tone, in which case the influence of impact damping on the simulated tone is apparent on the calculated spectrum. The necessity of such a model for simulating other types of instruments (or different acoustic systems) remains to be investigated using both a numerical and a perceptual approach.

Including two types of damping in this study (parameterised using γ and r) provides a framework for the treatment of a wide range of lumped systems involving nonlinear interactions. An interesting extension of the presented convergence study would be to analyse distributed systems, such as a string interacting with a barrier (see, e.g. [7, 8, 10, 13]). For such systems the nonlinear equation to be solved is a vector equation of the form

$$\mathbf{F}(\mathbf{x}) = \mathbf{0}. \tag{37}$$

In this case a direct analysis of Newton's method is more involved. However (37) could be interpreted as a fixed-point iteration problem $\mathbf{x} = \mathbf{T}(\mathbf{x})$, where the Lipschitz constant of $\mathbf{T}$ [26] relates to the number of required iterations until convergence to the solution $\mathbf{x}^*$ is achieved.

6. ACKNOWLEDGMENTS

This research is supported by the Austrian Science Fund (FWF): P28655-N32. S. Bilbao was supported by the European Research Council, under grant 2011-StG-279068-NESS.

7. REFERENCES

[1] A. Chaigne and J. Kergomard, *Acoustics of Musical Instruments*, Springer, New York, 2016.

[2] V. Chatziioannou and M. van Walstijn, "An energy conserving finite difference scheme for simulation of collisions," in *Sound and Music Computing (SMAC-SMC 2013)*, Stockholm, 2013, pp. 584–591.

[3] S. Bilbao, A. Torin, and V. Chatziioannou, "Numerical modeling of collisions in musical instruments," *Acta Acustica united with Acustica*, vol. 101, no. 1, pp. 155–173, 2015.

[4] M. Ducceschi, S. Bilbao, and C. Desvages, "Modelling collisions of nonlinear strings against rigid barriers: Conservative finite difference schemes with application to sound synthesis," in *International Congress on Acoustics*, Buenos Aires, 2016.

[5] S. Bilbao, *Numerical Sound Synthesis*, Wiley & Sons, Chichester, UK, 2009.

[6] G. Evangelista and F. Eckerholm, "Player-instrument interaction models for digital waveguide synthesis of guitar: Touch and collisions," *IEEE Transactions on Audio, Speech and Language Processing*, vol. 18, no. 4, pp. 822–832, 2010.

[7] M. van Walstijn and J. Bridges, "Simulation of distributed contact in string instruments: a modal expansion approach," in *Europ. Sig. Proc Conf (EUSIPCO2016)*, 2016, pp. 1023–1027.

[8] C. Issanchou, S. Bilbao, J. Le Carrou, C. Touzé, and O. Doaré, "A modal-based approach to the nonlinear vibration of strings against a unilateral obstacle: Simulations and experiments in the pointwise case," *Journal of Sound and Vibration*, vol. 393, pp. 229–251, 2017.

[9] K. Hunt and F. Crossley, "Coefficient of restitution interpreted as damping in vibroimpact," *Journal of Applied Mechanics*, vol. 42, pp. 440–445, 1975.

[10] M. van Walstijn and V. Chatziioannou, "Numerical simulation of tanpura string vibrations," in *Proc. International Symposium on Musical Acoustics, Le Mans*, 2014, pp. 609–614.

[11] C. Desvages and S. Bilbao, "Two-polarisation physical model of bowed strings with nonlinear contact and friction forces, and application to gesture-based sound synthesis," *Applied Sciences*, vol. 6, no. 5, 2016.

[12] S. Papetti, F. Avanzini, and D. Rocchesso, "Numerical methods for a nonlinear impact model: A Comparative study with closed-form corrections," *IEEE Transactions on Audio, Speech and Language Processing*, vol. 19, no. 7, pp. 2146–2158, 2011.

[13] V. Chatziioannou and M. van Walstijn, "Energy conserving schemes for the simulation of musical instrument contact dynamics," *Journal of Sound and Vibration*, vol. 339, pp. 262–279, 2015.

[14] D.E. Hall, "Piano string excitation. VI: Nonlinear modeling," *Journal of the Acoustical Society of America*, vol. 92, no. 1, pp. 95–105, 1992.

[15] A. Chaigne and V. Doutaut, "Numerical simulation of xylophones. I. Time-domain modeling of the vibrating bars," *Journal of the Acoustical Society of America*, vol. 101, no. 1, pp. 539–557, 1997.

[16] T. Taguti, "Dynamics of simple string subject to unilateral constraint: A model analysis of sawari mechanism," *Acoustical science and technology*, vol. 29, no. 3, pp. 203–214, 2008.

[17] N. Lopes and T. Hélie, "Energy balanced model of a jet interacting with a brass player's lip," *Acta Acustica united with Acustica*, vol. 102, no. 1, pp. 141–154, 2016.

[18] V. Chatziioannou and M. Van Walstijn, "Discrete-time conserved quantities for damped oscillators," in *Proc. Third Vienna Talk on Music Acoustics*, 2015, pp. 135–139.

[19] A. Torin, *Percussion Instrument Modelling In 3D: Sound Synthesis Through Time Domain Numerical Simulation*, Ph.D. thesis, The University of Edinburgh, 2016.

[20] M. van Walstijn and F. Avanzini, "Modelling the mechanical response of the reed-mouthpiece-lip system of a clarinet. Part II. A lumped model appproximation," *Acustica*, vol. 93, no. 1, pp. 435–446, 2007.

[21] J.P. Dalmont, J. Gilbert, and S. Ollivier, "Nonlinear characteristics of single-reed instruments: Quasistatic volume flow and reed opening measurements," *Journal of the Acoustical Society of America*, vol. 114, no. 4, pp. 2253–2262, 2003.

[22] V. Chatziioannou and M. van Walstijn, "Estimation of clarinet reed parameters by inverse modelling," *Acta Acustica united with Acustica*, vol. 98, no. 4, pp. 629–639, 2012.

[23] E. Ducasse, "A physical model of a single-reed wind instrument, including actions of the player," *Computer Music Journal*, vol. 27, no. 1, pp. 59–70, 2003.

[24] A. Braden, D. Chadefaux, V. Chatziioannou, S. Siddiq, C. Geyer, S. Balasubramanian, and W. Kausel, "Acoustic Research Tool (ART)," `http://sourceforge.net/projects/artool`, 2006–2017.

[25] B. Gazengel, J. Gilbert, and N. Amir, "Time domain simulation of single reed wind instrument. From the measured input impedance to the synthesis signal. Where are the traps?," *Acta Acustica*, vol. 3, pp. 445–472, 1995.

[26] J. Ortega and W. Rheinboldt, *Iterative Solution of Nonlinear Equations in Several Variables*, vol. 30, SIAM, New York, 1970.

APPENDIX: BOUND ON NEWTON INTERATIONS

Starting from a user chosen x_0, one iteratively gets approximations to the solution of $F(x) = 0$ by

$$x_{k+1} = x_k - \frac{F(x_k)}{F'(x_k)}, \quad k = 0, 1, \ldots. \tag{38}$$

Let x^* denote the unique solution of $F(x) = 0$. Due to (31), we know that

$$F(x) > 0, \text{ for } x > x^*, \tag{39}$$
$$F(x) < 0, \text{ for } x < x^*. \tag{40}$$

First we assume that $x_0 < x^*$, hence $F(x_0) < 0$. It follows from (32), that

$$-F(x_0) = \int_{x_0}^{x^*} F'(x)dx \geq (x^* - x_0)F'(x_0), \tag{41}$$

hence

$$x_1 = x_0 - F(x_0)/F'(x_0) \geq x^*, \tag{42}$$

so after the first Newton step, we end up to the right of the solution x^*. On the other hand, starting from $x_0 > x^*$, we obtain

$$F(x_0) = \int_{x^*}^{x_0} F'(x)dx \leq (x_0 - x^*)F'(x_0), \tag{43}$$

hence

$$x^* \leq x_0 - F(x_0)/F'(x_0) = x_1. \tag{44}$$

In summary, starting Newton's method with an $x_0 > x^*$ yields a sequence $x_k, k = 0, 1, \ldots$ with $x_k > x^*$, whereas when starting with an $x_0 < x^*$ then $x_k > x^*$ for $k = 1, 2, \ldots$.

Furthermore, for $x_0 > x^*$, we observe that

$$F(x_0) = \int_{x^*}^{x_0} F'(x)dx \geq (x_0 - x^*)F'(x^*). \tag{45}$$

Therefore

$$0 \leq x_1 - x^* = (x_0 - x^*) - \frac{F(x_0)}{F'(x_0)} \tag{46}$$
$$\leq (x_0 - x^*) - \frac{(x_0 - x^*)F'(x^*)}{F'(x_0)} \tag{47}$$
$$= (x_0 - x^*)\left(1 - \frac{F'(x^*)}{F'(x_0)}\right) \tag{48}$$
$$\leq (x_0 - x^*)\left(1 - \frac{1}{F'(x_0)}\right) \tag{49}$$

We can now estimate the error in the kth step, $x_k - x^*$ by the initial error, using the fact that F' is an increasing function, and the sequence $x_k, k = 0, 1, \ldots$ is decreasing.

$$0 \leq x_k - x^* \leq (x_{k-1} - x^*)\left(1 - \frac{1}{F'(x_{k-1})}\right) \tag{50}$$
$$\leq (x_{k-1} - x^*)\left(1 - \frac{1}{F'(x_0)}\right) \tag{51}$$
$$\leq (x_0 - x^*)\left(1 - \frac{1}{F'(x_0)}\right)^k. \tag{52}$$

To finalise a priori estimates on the error $x_k - x^*$, we observe from (28b) that x^* is in the interval $[-B_x, B_x]$, hence $x_0 - x^* \leq 2B_x$, provided the starting point x_0 is taken from the same interval. Finally, we estimate

$$1 \leq F'(x_0) \leq F'(B_x). \tag{53}$$

The function F' depends on y^n as well,

$$\begin{aligned} F'(x, y^n) = &\left(1 + \frac{\gamma\Delta_t}{2}\right) + \frac{\Delta_t^2}{2m}\left(\frac{V'(y^n + x)}{x}\right) \\ &- \frac{\Delta_t^2}{2m}\left(\frac{V(y^n + x) - V(y^n)}{x^2}\right) \\ &+ \frac{r\Delta_t}{2m}\left(V_c'(y^n + x)\right). \end{aligned} \tag{54}$$

In order to get a bound independent of y^n , we observe that

$$\begin{aligned} \frac{\partial}{\partial y^n}F'(x, y^n) = &\frac{\Delta_t^2}{2m}\frac{V''(y^n + x)}{x} \\ &- \frac{\Delta_t^2}{2m}\frac{V'(y^n + x) - V'(y^n)}{x^2} \\ &+ \frac{r\Delta_t}{2m}V_c''(y^n + x) \geq 0 \end{aligned} \tag{55}$$

Using the fact that V' is convex, it can be shown that

$$F'(B_x, y^n) \leq F'(B_x, B_y), \tag{56}$$

where B_y is given by (29), hence for $x_0 \geq x^*$,

$$0 \leq x_k - x^* \leq 2B_x\left(1 - \frac{1}{F'(B_x, B_y)}\right)^k. \tag{57}$$

To achieve a given precision ε, one needs to perform at most

$$k = \frac{\log\varepsilon - \log(2B_x)}{\log\left(1 - \frac{1}{F'(B_x, B_y)}\right)} \tag{58}$$

Newton steps. For $x_0 \leq x^*$, one needs to perform at most $k + 1$ steps, since $x_1 \geq x^*$, and if x_1 exceeds B_x, one should set $x_1 = B_x$.